

Unconventional Spin Density Wave in $(\text{TMTSF})_2\text{PF}_6$ below $T^* \approx 4$ K

Mario Basletić*

Department of Physics, Faculty of Science, POB 331, HR-10002 Zagreb, Croatia

Bojana Korin-Hamzić

Institute of Physics, POB 304, HR-10001 Zagreb, Croatia

Kazumi Maki

*Department of Physics, University of Southern California,
Los Angeles CA 90089-0484, USA*

and

*Max-Planck Institute for the Physics of Complex Systems,
Nöthnitzer Str.38, D-01187 Dresden, Germany*

(Dated: November 2, 2018)

The presence of subphases in spin-density wave (SDW) phase of $(\text{TMTSF})_2\text{PF}_6$ below $T^* \approx 4$ K has been suggested by several experiments but the nature of the new phase is still controversial. We have investigated the temperature dependence of the angular dependence of the magnetoresistance in the SDW phase which shows different features for temperatures above and below $T^* \approx 4$ K. For $T > 4$ K the magnetoresistance can be understood in terms of the Landau quantization of the quasiparticle spectrum in a magnetic field, where the imperfect nesting plays the crucial role. We propose that below $T^* \approx 4$ K the new unconventional SDW (USDW) appears modifying dramatically the quasiparticle spectrum. Unlike conventional SDW the order parameter of USDW depends on the quasiparticle momentum $\Delta_1(\mathbf{k}) \propto \cos 2bk_y$. The present model describes many features of the angular dependence of magnetoresistance reasonably well. Therefore, we may conclude that the subphase in $(\text{TMTSF})_2\text{PF}_6$ below $T^* \approx 4$ K is described as SDW plus USDW.

PACS numbers: 72.15.Gd, 74.70.Kn, 71.70.Di

I. INTRODUCTION

The very anisotropic organic conductors $(\text{TMTSF})_2\text{X}$ (where TMTSF is tetramethyltetraselenafulvalene and $\text{X} = \text{PF}_6, \text{AsF}_6, \text{ClO}_4 \dots$ stands for monovalent anion) or Bechgaard salts continue to attract much attention since the discovery of their superconductivity in 1979.¹ A variety of electronic ground states under pressure and/or magnetic field, (conventional) spin density wave (SDW), field induced spin density wave (FISDW) with quantum Hall effect and unconventional (most likely p -wave) superconductivity, are very intriguing.^{2,3}

$(\text{TMTSF})_2\text{PF}_6$ is metallic down to $T_{\text{SDW}} \approx 12$ K, where the transition into the semiconducting SDW state occurs. It is known that SDW in $(\text{TMTSF})_2\text{PF}_6$ undergoes another transition at $T^* \approx T_{\text{SDW}}/3$ (at 3.5–4 K at ambient pressure).^{4,5,6} The indication of the subphase transition was first seen by NMR,⁴ where T_1^{-1} diverges and the spin susceptibility changes at T^* . The transition at T^* is preserved through the entire $P - T$ phase diagram. Furthermore, a calorimetric transition at 3.5 K, with a large hysteretic phenomena in the temperature range 2.5–4 K (caused by the sample history), has been observed and interpreted as an indication of a glass transition.⁶ On the other hand, the low frequency dielectric relaxation of SDW in $(\text{TMTSF})_2\text{PF}_6$ did not show the existence of the glass transition.⁷ Since then, the SDW state was widely investigated, but the nature of the possible subphases remains controversial. Our study of

the angular dependence of the magnetoresistance (MR) for $\mathbf{B} \parallel (\mathbf{a} - \mathbf{b}')$ plane has shown dramatically different features above and below $T^* \approx 4$ K.^{8,9} However, taking into account our MR results for temperatures $T \geq 2.2$ K, the transition at T^* appears to be unique to $(\text{TMTSF})_2\text{PF}_6$, as it has not been identified for $\text{X} = \text{AsF}_6$ and ClO_4 .¹⁰ On the other hand, there are a few reports^{11,12} indicating similar transition in $(\text{TMTSF})_2\text{AsF}_6$, though less pronounced than in $(\text{TMTSF})_2\text{PF}_6$. Therefore, at this moment, we cannot exclude the presence of similar transitions in other Bechgaard salts.

Recently, we have studied the MR in $(\text{TMTSF})_2\text{PF}_6$, with a magnetic field rotated within the $\mathbf{a} - \mathbf{c}^*$ plane, which behaves differently for $T > 4$ K and $T < 4$ K at ambient pressure.¹³ For $T > 4$ K the magnetoresistance was described in terms of the quasiparticles scattered by the \mathbf{k} dependent scattering rate (where \mathbf{k} is the quasiparticle wave vector). In other words, we could understand the magnetotransport in terms of the standard Fermi liquid theory, i.e. by the quasiparticles with the energy gap given in the model with imperfect nesting.¹⁴ In spite of the fact that for $T < 4$ K we had to introduce a rather artificial scattering rate $\Gamma(\phi = bk_y)$ the description of the resistance along the \mathbf{b}' axis was not satisfactory.¹³

More recently, an unconventional density wave (USDW and UCWD) was proposed as a possible ground state of the electronic systems in organic conductors and heavy fermion systems.^{15,16,17,18,19} Unlike the conventional SDW, the USDW is defined as the SDW where the order parameter $\Delta(\mathbf{k})$ depends on the quasi-particle

momentum \mathbf{k} . In spite of a clear thermodynamic signal (as in the usual mean field-like transition), the first order term in $\Delta(\mathbf{k})$, corresponding to local charge or local spin, is invisible. Consequently, these states may be called the phase with hidden order parameter.¹⁹ UCWD has been identified very recently, from the temperature dependence of the threshold electric field,²⁰ in the low temperature phase of α -(ET)₂KHg(SCN)₄.²¹ Similarly, a mysterious micromagnetism seen in AF phase of URu₂Si₂ could also be interpreted in terms of USDW.²²

The aim of this work was to see if the presence of possible subphases in the SDW below 4 K could be observed in the temperature dependence of the conductivity and MR as well as in the anisotropy of the MR. In this paper we compare the experimental MR data of (TMTSF)₂PF₆ in the SDW state, showing the pronounced differences for $T > 4$ K and $T < 4$ K, with our new theoretical results (preliminary results in Ref. 23). We propose that the anomaly at $T^* \approx 4$ K in (TMTSF)₂PF₆ signals the appearance of USDW. We point out that USDW requires more subtle balance between different interaction terms than conventional SDW,¹⁵ and consequently it is perhaps not easily found in other Bechgaard salts.

II. EXPERIMENT.

The measurements were done down to 2 K in magnetic fields up to 5 T and with different directions of the current (through the crystal) and different orientations of magnetic field. A rotating sample holder enabled the sample rotation around a chosen axis over a range of 190°. The single crystals used come all from the same batch. Their \mathbf{a} direction is the highest conductivity direction, the \mathbf{b}' direction (with intermediate conductivity) is perpendicular to \mathbf{a} in the $\mathbf{a}-\mathbf{b}$ plane and \mathbf{c}^* direction (with the lowest conductivity) is perpendicular to the $\mathbf{a}-\mathbf{b}$ (and $\mathbf{a}-\mathbf{b}'$). The room temperature conductivity values for $\sigma_{\mathbf{a}}$, $\sigma_{\mathbf{b}}$, and $\sigma_{\mathbf{c}}$ are 500 ($\Omega \text{ cm}$)⁻¹, 20 ($\Omega \text{ cm}$)⁻¹, and 1/35 ($\Omega \text{ cm}$)⁻¹ respectively.

The experimental MR data, that will be analyzed here, are for \mathbf{c}^* and \mathbf{b}' axis and for different orientations of magnetic field. The MR, defined as $\Delta\rho/\rho_0 = [\rho(B) - \rho(0)]/\rho(0)$, was measured in various four probe arrangements on samples cut from a long crystal. Moreover, the measurements of \mathbf{c}^* axis MR, for two different magnetic field rotations, were performed on the same sample but which was cut to two parts. In the case of $\rho_{\mathbf{b}}$ ($\mathbf{j} \parallel \mathbf{b}'$) two pairs of the contacts were placed on the opposite $\mathbf{a}-\mathbf{c}^*$ surfaces while for $\rho_{\mathbf{c}}$ ($\mathbf{j} \parallel \mathbf{c}^*$) on the opposite $\mathbf{a}-\mathbf{b}'$ surfaces. We used very slow cooling rates (about 2–5 K per hour) to avoid the appearance of the irreversible resistance jumps usually encountered for $\mathbf{j} \parallel \mathbf{a}$ measurements. This was especially important for $\mathbf{j} \parallel \mathbf{b}'$ geometry, where additional care was required to avoid possible mixture of $\sigma_{\mathbf{b}}$ and $\sigma_{\mathbf{c}}$ conductivities.¹³ This can be described by using the concept of the equivalent isotropic sample that gives a simple picture of the current distri-

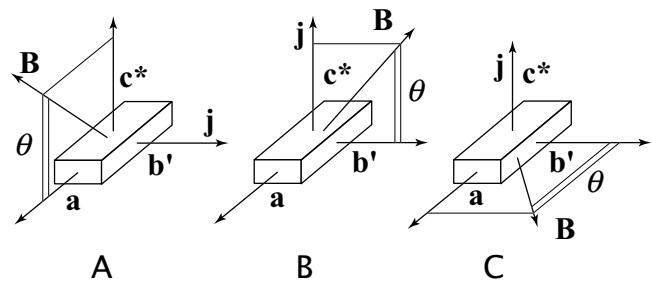


FIG. 1: Three configurations (case A, B and C) of the current \mathbf{j} and magnetic field \mathbf{B} direction. (See text for a detailed explanation.)

bution in the anisotropic sample.²⁴ The eligible test for properly measured \mathbf{b}' -axis resistivity is linear temperature dependence at high temperatures.²⁵ Namely, there is a non-monotonic temperature dependence of $\rho_{\mathbf{c}}$ in (TMTSF)₂PF₆ at ambient pressure going through a well characterized maximum at 80 K in contrast to the results for $\rho_{\mathbf{a}}$ ($\propto T^2$) and $\rho_{\mathbf{b}}$ ($\propto T$) exhibiting a monotonous, metallic-like decrease upon lowering temperature.

Figure 1 present three configurations that will be analyzed in this work: a) Fig. 1A shows the case when the current direction is along the \mathbf{b}' axis and the magnetic field is rotated in the $\mathbf{a}-\mathbf{c}^*$ ($\mathbf{j} \parallel \mathbf{b}'$, $\mathbf{B} \parallel (\mathbf{a}-\mathbf{c}^*)$) perpendicular to the current direction. θ is the angle between \mathbf{B} and the \mathbf{a} axis, i.e. $\theta = 0$ for $\mathbf{B} \parallel \mathbf{a}$ and $\theta = 90^\circ$ for $\mathbf{B} \parallel \mathbf{c}^*$. b) Fig. 1B shows the case when the current direction is along the \mathbf{c}^* axis and the magnetic field is rotated in the $\mathbf{b}'-\mathbf{c}^*$ plane ($\mathbf{j} \parallel \mathbf{c}^*$, $\mathbf{B} \parallel (\mathbf{b}'-\mathbf{c}^*)$). θ is the angle between \mathbf{B} and the \mathbf{b}' axis, i.e. $\theta = 0$ for $\mathbf{B} \parallel \mathbf{b}'$ and $\theta = 90^\circ$ for $\mathbf{B} \parallel \mathbf{c}^*$. c) Fig. 1C shows the case when the current direction is along the \mathbf{c}^* axis and the magnetic field is rotated in the $\mathbf{a}-\mathbf{b}'$ plane ($\mathbf{j} \parallel \mathbf{c}^*$, $\mathbf{B} \parallel (\mathbf{a}-\mathbf{b}')$) perpendicular to the current direction. θ is the angle between \mathbf{B} and the \mathbf{b}' axis, i.e. $\theta = 0$ for $\mathbf{B} \parallel \mathbf{b}'$ and $\theta = 90^\circ$ for $\mathbf{B} \parallel \mathbf{a}$.

III. MODEL, RESULTS AND DISCUSSION.

A. Quasiparticle spectrum above $T^* \approx 4$ K.

We limit ourselves to the \mathbf{c}^* axis magnetoresistance, i.e. to the case B when the current \mathbf{j} direction is along the \mathbf{c}^* axis, the magnetic field is rotated in the $\mathbf{b}'-\mathbf{c}^*$ plane with $\theta = \angle(\mathbf{b}', \mathbf{B})$. We leave a detailed analysis for another current directions and magnetic field orientations above 4 K for a future publication.

The Landau quantization of the quasiparticle spectrum appears to describe very well the observed results. In the limit of perfect nesting all the electron orbits are open and there will be no Landau quantization. On the other hand, in the presence of the imperfect nesting¹⁴ as in (TMTSF)₂PF₆ the quasiparticle energy landscape develops local minima at $k_z = \pm k_F$, $k_y = \pm \pi/2b$. In other words, closed orbits appear and they will be quantized in

the presence of a magnetic field.

For $T > 4$ K the quasiparticle energy is given by:¹³

$$\begin{aligned} E_{\mathbf{k}} &= \sqrt{\eta^2 + \Delta^2} - \varepsilon_0 \cos 2bk_y \\ &\approx \Delta - \varepsilon_0 + \frac{1}{2\Delta}\eta^2 + 2\varepsilon_0 b^2 k_y^2, \end{aligned} \quad (1)$$

where $\eta = [v_a^2(k_x - k_F)^2 + v_c^2 k_z^2]^{1/2}$ is the quasiparticle energy in the normal state (v_a and v_c are Fermi velocities in \mathbf{a} and \mathbf{c}^* direction, respectively), Δ (≈ 34 K) is the order parameter for conventional SDW and ε_0 (≈ 13 K) is the parameter characterizing the imperfect nesting effect.¹³ The quasiparticle energy is expanded for small $(k_x - k_F)^2$ and k_z^2 . In a presence of a magnetic field within the \mathbf{b}' - \mathbf{c}^* plane, with θ being the angle between the magnetic field \mathbf{B} and the \mathbf{b}' axis, the minimum energy (i.e. the energy gap) in Eq. (1) is given by:

$$E(B, \theta) \approx \Delta - \varepsilon_0 + \sqrt{\frac{\varepsilon_0}{\Delta} v_a b e B \sqrt{\sin^2 \theta + \gamma_2 \cos^2 \theta}}, \quad (2)$$

with $\gamma_2 = (1/\varepsilon_0 \Delta)(v_c/2b)^2$. For $B = 0$ the resistance is given as $\rho_{zz}(T, 0) \propto \exp[\beta E(0, \theta)]$, whereas for $B \neq 0$ we have:

$$\rho_{zz}(T, B) \propto B \sqrt{\sin^2 \theta + \gamma_2 \cos^2 \theta} e^{\beta E(B, \theta)}. \quad (3)$$

First, we note that the energy gap is given in the both limits ($B = 0$ and $B \neq 0$) by Eq. (2). Second, for $\omega_c \tau > 1$, where ω_c is the cyclotron frequency and τ is the scattering rate, $\rho_{zz}(T, B)$ contains a B linear coefficient. So, we may interpolate these expressions as:

$$\begin{aligned} \rho_{zz}(B, T) &\approx e^{\beta(\Delta - \varepsilon_0)} (1 + A_2 B \sqrt{\sin^2 \theta + \gamma_2 \cos^2 \theta}) \\ &\times \left(1 + C_2 B \sqrt{\sin^2 \theta + \gamma_2 \cos^2 \theta} \right), \end{aligned} \quad (4)$$

with $A_2 = (\varepsilon_0/\Delta)^{1/2} v_a b e / (\Delta - \varepsilon_0)$.

We shall compare now our experimental data with the above equations. The magnetic field dependence of MR for $\mathbf{j} \parallel \mathbf{c}^*$, $\mathbf{B} \parallel \mathbf{b}'$ and $\mathbf{B} \parallel \mathbf{c}^*$ at 4.2 K is presented in Fig. 2. Fig. 3 shows the angular dependence of MR for $\mathbf{j} \parallel \mathbf{c}^*$, $B = 5$ T at 4.2 K and 2.2 K. θ is the angle between \mathbf{B} and the \mathbf{b}' axis (see Fig. 1, case B). Solid line is the fit based on the Eq. (4). The change in the angular dependence of MR for $T > 4$ K and $T < 4$ K is clearly seen (the case for $T = 2.2$ K will be treated in Section III B). It is evident that the present model describes rather well the data, with both the field and angular dependence of MR, at $T = 4.2$ K and $B = 5$ T giving $(\Delta - \varepsilon_0) = 21$ K, $A_2 = 0.014$ T⁻¹, $C_2 = 0.38$ T⁻¹ and $\gamma_2 = 0.85$. These values enable us to extract the \mathbf{a} axis coherence length $\xi_a = v_a/\Delta = 1.2 \times 10^{-6}$ cm and $v_c/v_a = 7.33 \times 10^{-2}$ (we

used here flux quantum $\pi/e = \Phi_0 = 2.07 \times 10^{-11}$ T cm²). Both ξ_a and v_c/v_a thus deduced are consistent with the ones deduced from the anisotropy in the resistivity.²

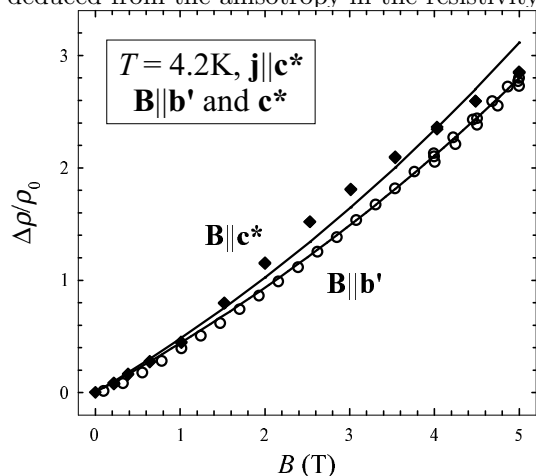


FIG. 2: Magnetic field dependence of $\Delta\rho/\rho_0$ at 4.2 K for $\mathbf{j} \parallel \mathbf{c}^*$, $\mathbf{B} \parallel \mathbf{b}'$ and $\mathbf{B} \parallel \mathbf{c}^*$. Solid lines are fits to the theory (see text).

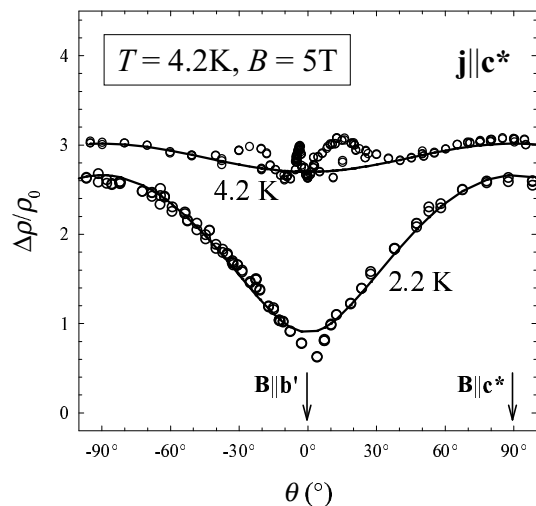


FIG. 3: Angular dependence of $\Delta\rho/\rho_0$ at 2.2 K and 4.2 K, $B = 5$ T, for $\mathbf{j} \parallel \mathbf{c}^*$, \mathbf{B} in \mathbf{b}' - \mathbf{c}^* plane. Solid lines are fits to the theory (see text).

B. Quasiparticle spectrum below $T^* \approx 4$ K.

We start by proposing that the anomaly at $T^* \approx 4$ K in (TMTSF)₂PF₆ signals the appearance of USDW with the momentum dependent order parameter $\Delta_1(\mathbf{k}) = \Delta_1 \cos 2\phi$, where $\phi = bk_2$ with wave vector $\mathbf{Q} = (2k_F, \pi/2b, 0)$. In other words, below T^* two order parameters (SDW and USDW) coexist. In this case the quasiparticle spectrum changes from Eq. (1) to:

$$E_{\mathbf{k}} = \sqrt{\left(\sqrt{\eta^2 + \Delta^2} - \varepsilon_0 \cos 2bk_y\right)^2 + \Delta_1^2 \cos^2 2\phi} \quad (5)$$

$$\begin{aligned} &= \sqrt{(\eta^2 + \Delta^2) \frac{\Delta_1^2}{\Delta_1^2 + \varepsilon_0^2} + (\Delta_1^2 + \varepsilon_0^2) (\cos^2 2\phi - \cos^2 2\phi_0)^2} \\ &\approx \sqrt{\tilde{\Delta}^2 + \tilde{v}_a^2 (k_x - k_F)^2 + \tilde{v}_c^2 k_z^2 + 4(\Delta_1^2 + \varepsilon_0^2) b^2 k_y^2}, \end{aligned} \quad (6)$$

where $\tilde{\Delta}^2 = \Delta \Delta_1 (\Delta_1^2 + \varepsilon_0^2)^{-1/2}$, $\tilde{v}_a = v_a \Delta_1 (\Delta_1^2 + \varepsilon_0^2)^{-1/2}$ and $\tilde{v}_c = v_c \Delta_1 (\Delta_1^2 + \varepsilon_0^2)^{-1/2}$. We have not included a constant shift in k_y and k_z , since they are of no importance when one considers the effect of the magnetic field. In the absence of the magnetic field, the effect of Δ_1 (or USDW) is to change the minimum energy gap from $E_{\min} = \Delta - \varepsilon_0$ ($T > 4$ K) to $E_{\min} = \tilde{\Delta}$ ($T < 4$ K). As we shall see later, the introduction of the magnetic field changes dramatically the minimum energy gap E_{\min} . Such a dramatic shift in E_{\min} in USDW and UCDW in a magnetic field has already been discussed in Ref. 26 and 16.

We shall see in the following that the field and the angle dependent quasiparticle spectrum describes the angle dependent MR observed in $(\text{TMTSF})_2\text{PF}_6$ below $T^* \approx 4$ K rather satisfactory. The quasiparticle energy gap in the absence of magnetic field is given by Eqs. (5) and (6). Due to the quadratic form in \mathbf{k} in the square root, we expect the Landau quantization in the presence of magnetic field. Let us consider three cases (Fig. 1) separately.

1. *Case A: $\mathbf{j} \parallel \mathbf{b}'$, $\mathbf{B} \parallel (\mathbf{a} - \mathbf{c}^*)$, $\theta = \angle(\mathbf{a}, \mathbf{B})$*

We can recast Eq. (6) as an eigenvalue problem:

$$\begin{aligned} E^2(B, \theta)\psi &= \left[\tilde{\Delta}^2 + \tilde{v}_a^2 (eBy \cos \theta)^2 + \tilde{v}_c^2 (eBy \sin \theta)^2 \right. \\ &\quad \left. - (2b)^2 (\Delta_1^2 + \varepsilon_0^2) \frac{d^2}{dy^2} \right] \psi, \end{aligned} \quad (7)$$

where ψ is the electron wave function. This gives readily for the quasiparticle energy corresponding to the n -th Landau level:

$$E_n^2(B, \theta) = \tilde{\Delta}^2 + 2\tilde{v}_a \Delta_1 eB (\sin^2 \theta + \gamma_1 \cos^2 \theta)^{1/2} (2n + 1), \quad (8)$$

($n = 0, 1, 2, \dots$). From this we obtain the minimum energy gap E_{\min} :

$$E_{\min}(B, \theta) = \tilde{\Delta} \sqrt{1 + A_1 |B| (\sin^2 \theta + \gamma_1 \cos^2 \theta)^{1/2}}, \quad (9)$$

$$A_1 = \frac{2\tilde{v}_a \Delta_1}{\tilde{\Delta}^2} be, \quad \gamma_1 = \left(\frac{\tilde{v}_c}{\tilde{v}_a} \right)^2 \sim 10^{-3}.$$

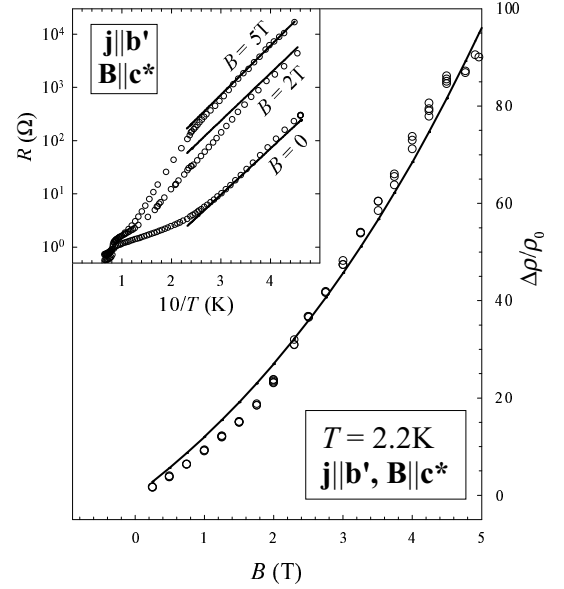


FIG. 4: Magnetic field dependence of $\Delta\rho/\rho_0$ at 2.2 K for $\mathbf{j} \parallel \mathbf{b}'$ and $\mathbf{B} \parallel \mathbf{c}^*$. Inset: R vs. inverse temperature for $B = 0, 2$ T, and 5 T. Solid lines are fits to the theory (see text).

In this configuration γ_1 is clearly negligible. By approximating the cyclotron frequency as:

$$\begin{aligned} E_1(B, \theta) - E_0(B, \theta) &= \\ &= \tilde{\Delta} \left(\sqrt{1 + 3A_1 |B \sin \theta|} - \sqrt{1 + A_1 |B \sin \theta|} \right) \\ &\approx \tilde{\Delta} A_1 |B \sin \theta|, \end{aligned} \quad (10)$$

and noting the fact that in the presence of magnetic field

$$\sigma_{yy} \approx \frac{|B \sin \theta| \exp \left[-\beta \tilde{\Delta} \sqrt{1 + A_1 |B \sin \theta|} \right]}{1 + C' (B \sin \theta)^2},$$

we finally obtain the interpolation formula:

$$\begin{aligned} \rho_{yy} &\approx \exp \left(\beta \tilde{\Delta} \sqrt{1 + A_1 |B \sin \theta|} \right) \\ &\quad \times (1 + C_1 A_1 |B \sin \theta|), \end{aligned} \quad (11)$$

where $C_1 = (\tilde{\Delta}/\Gamma)^2$ and Γ is the quasiparticle relaxation rate (note that Γ is \mathbf{k} -independent).

The comparison of Eq. (11) (with $\theta = \pi/2$) with the experimental data is given in Figs. 4 and 5. Fig. 4 shows

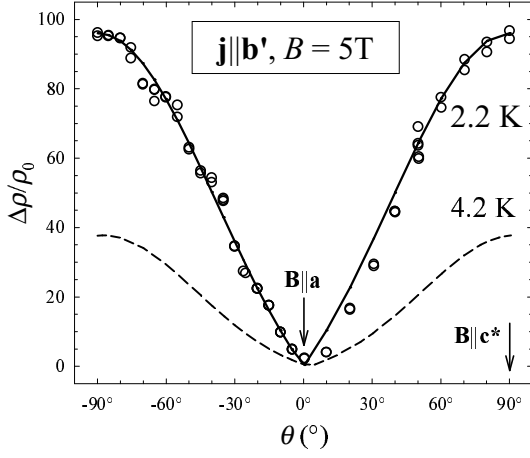


FIG. 5: Angular dependence of $\Delta\rho/\rho_0$ at 2.2 K and 4.2 K, $B = 5$ T, for $\mathbf{j}\parallel\mathbf{b}'$, \mathbf{B} in $\mathbf{a}-\mathbf{c}^*$ plane. Solid line is fit to the theory (see text).

the results of the magnetic field dependence of the MR at 2.2 K for $\mathbf{j}\parallel\mathbf{b}'$ and $\mathbf{B}\parallel\mathbf{c}^*$. The inset shows the temperature dependence of the MR for $B = 5$ T in the same geometry. The solid lines show the fit to the theoretical model explained above. Fig. 5 shows the angular dependence of MR for $\mathbf{j}\parallel\mathbf{b}'$ and $B = 5$ T at 2.2 K (see Fig. 1, case A). Dashed line shows the results at 4.2 K. Solid line is fit based on Eq. (11). Further, the $1/T$ dependent magnetoresistance is compared in the inset of Fig. 4. By fitting the data we can deduce $\tilde{\Delta} = 20$ K, $A_1 = 0.027$ T $^{-1}$ which gives $\Delta_1/\tilde{\Delta} = 0.568$ (where we took $b = 0.77$ nm and $\xi_a = \tilde{v}_a/\tilde{\Delta} = 120$ Å). We obtain the USDW order parameter $\Delta_1 \approx 20$ K. These numbers look rather reasonable. So, in this geometry, the present model describes the experimental data reported in Ref. 13 rather well.

2. Case B: $\mathbf{j}\parallel\mathbf{c}^*$, $\mathbf{B}\parallel(\mathbf{b}'-\mathbf{c}^*)$, $\theta = \angle(\mathbf{b}', \mathbf{B})$

In this configuration the eigenequation is rewritten as:

$$E^2(B, \theta)\psi = \left[\tilde{\Delta}^2 - \tilde{v}_a^2 \frac{d^2}{dy^2} + \tilde{v}_c^2 (eBx \cos \theta)^2 + (2b)^2 (\Delta_1^2 + \varepsilon_0^2) (eBx \sin \theta)^2 \right] \psi, \quad (12)$$

which is solved as:

$$E_n^2(B, \theta) = \tilde{\Delta}^2 + 2\tilde{v}_a \Delta_1 eB (\sin^2 \theta + \gamma_2 \cos^2 \theta)^{1/2} (2n + 1), \quad (13)$$

($n = 0, 1, 2, \dots$). Therefore, the minimum energy gap E_{\min} is:

$$E_{\min}(B, \theta) = \tilde{\Delta} \sqrt{1 + A_2 |B| (\sin^2 \theta + \gamma_2 \cos^2 \theta)^{1/2}}, \quad (14)$$

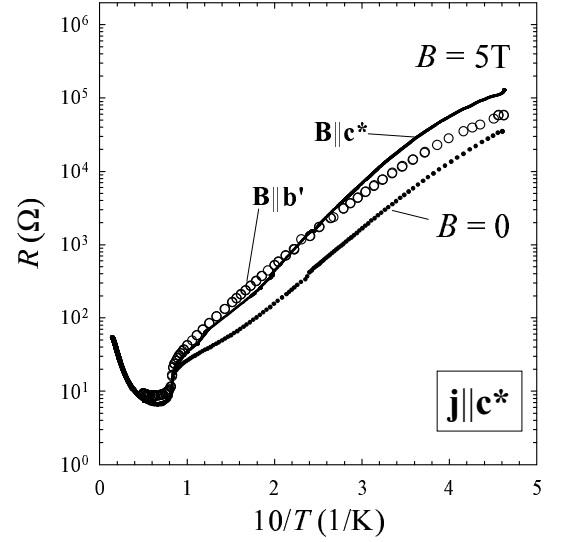


FIG. 6: Temperature dependence of the resistance R for $\mathbf{j}\parallel\mathbf{c}^*$, $B = 0$ and $B = 5$ T (for two different magnetic field orientations $\mathbf{B}\parallel\mathbf{b}'$ and $\mathbf{B}\parallel\mathbf{c}^*$).

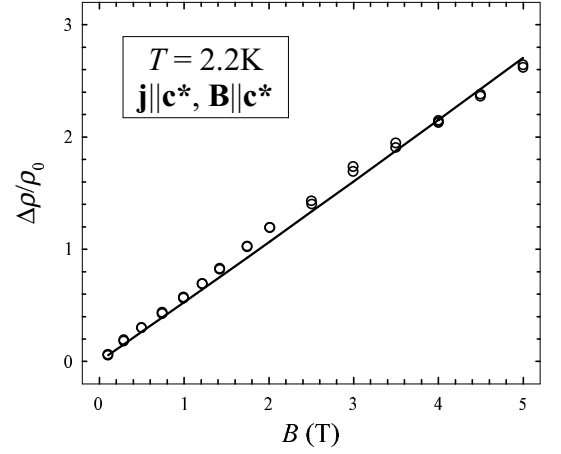


FIG. 7: Magnetic field dependence of $\Delta\rho/\rho_0$ at 2.2 K for $\mathbf{j}\parallel\mathbf{c}^*$ and $\mathbf{B}\parallel\mathbf{c}^*$. Solid line is fit to the theory (see text).

$$A_2 = \frac{2\tilde{v}_a \Delta_1}{\tilde{\Delta}^2} b e, \quad \gamma_2 = \frac{\tilde{v}_c^2}{(2b)^2 (\Delta_1^2 + \varepsilon_0^2)}.$$

The magnetoresistance along the \mathbf{c}^* axis is given by:

$$\rho_{zz} \approx \exp \left[\beta \tilde{\Delta} \sqrt{1 + A_2 |B| (\sin^2 \theta + \gamma_2 \cos^2 \theta)^{1/2}} \right] \times \left(1 + C_2 A_2 |B| \sqrt{\sin^2 \theta + \gamma_2 \cos^2 \theta} \right). \quad (15)$$

Figure 6 shows the temperature dependence of the resistance for $\mathbf{j}\parallel\mathbf{c}^*$ ($B = 0$, $B = 5$ T) and for two different magnetic field orientations $\mathbf{B}\parallel\mathbf{b}'$ and $\mathbf{B}\parallel\mathbf{c}^*$. The difference in R vs. $10/T$ behaviour below ≈ 4 K for two magnetic field orientations is clearly observed. The magnetic field dependence of magnetoresistance for $\mathbf{j}\parallel\mathbf{c}^*$ and

$\mathbf{B} \parallel \mathbf{c}^*$ at 2.2 K is presented in Fig. 7. As mentioned before, Fig. 3 shows also the angular dependence of magnetoresistance for $\mathbf{j} \parallel \mathbf{c}^*$, $B = 5$ T at 2.2 K (see Fig. 1, case B). Solid line (on both Fig. 3 and Fig. 7) is fit based on the Eq. (15). The present expression is comparable with both the B dependence of magnetoresistance for $\theta = \pi/2$ and the θ dependent magnetoresistance at $T = 2.2$ K and $B = 5$ T. Again, the present model describes the data rather well. In the present comparison we deduce $A_2 = 0.00134 \text{ T}^{-1} = A_1/20.2$, $C_2 = 0.5192 \text{ T}^{-1} = C_1/20.2$, and $\gamma_2 = 0.060$ which gives $\tilde{\Delta} = 20$ K and $v_c/v_a = 0.02$. On the other hand, we obtain $\Delta_1/\Delta = 0.0284$ that gives $\Delta_1 \approx 1$ K. This implies the USDW order parameter in the present configuration is reduced by a factor of 1/20 compared with the one in the first configuration. This result is rather unexpected, but we hope the future work will clarify this problem.

3. Case C: $\mathbf{j} \parallel \mathbf{c}^*$, $\mathbf{B} \parallel (\mathbf{a}-\mathbf{b}')$, $\theta = \angle(\mathbf{b}', \mathbf{B})$

In this configuration the eigenequation is rewritten as:

$$E^2(B, \theta)\psi = \left[\tilde{\Delta}^2 - \tilde{v}_c^2 \frac{d^2}{dz^2} + \tilde{v}_a^2 (eBz \sin \theta)^2 + (2b)^2 (\Delta_1^2 + \varepsilon_0^2) (eBz \cos \theta)^2 \right] \psi, \quad (16)$$

which gives

$$E_n^2(B, \theta) = \tilde{\Delta}^2 + 2\tilde{v}_c \tilde{v}_a eB (\sin^2 \theta + \gamma_3 \cos^2 \theta)^{1/2} (2n + 1), \quad (17)$$

($n = 0, 1, 2, \dots$). For the minimum energy gap E_{\min} we obtain:

$$E_{\min}(B, \theta) = \tilde{\Delta} \sqrt{1 + A_3 |B| (\sin^2 \theta + \gamma_3 \cos^2 \theta)^{1/2}}, \quad (18)$$

$$A_3 = \frac{\tilde{v}_a \tilde{v}_c e}{\tilde{\Delta}^2} b e, \quad \gamma_3 = \frac{(2b)^2 (\Delta_1^2 + \varepsilon_0^2)}{\tilde{v}_a^2}.$$

It follows that the magnetoresistance along the \mathbf{c}^* is given by:

$$\rho_{zz} \approx \exp \left[\beta \tilde{\Delta} \sqrt{1 + A_3 |B| (\sin^2 \theta + \gamma_3 \cos^2 \theta)^{1/2}} \right] \times \left(1 + C_3 A_3 |B| \sqrt{\sin^2 \theta + \gamma_3 \cos^2 \theta} \right). \quad (19)$$

Figure 8 presents the magnetic field dependence of MR for $\mathbf{j} \parallel \mathbf{c}^*$ and $\mathbf{B} \parallel \mathbf{a}$ at 2.2 K, while Fig. 9 shows the angular dependence of magnetoresistance for $\mathbf{j} \parallel \mathbf{c}^*$, $B = 5$ T at 2.2 K (see Fig. 1, case C). We point out that there is a maxima in MR for $\mathbf{B} \parallel \mathbf{a}$ at 2.2 K, while there is a minima in MR for $\mathbf{B} \parallel \mathbf{a}$ at 4.2 K (dashed line Fig. 9). This kind of behaviour cannot be described in terms of

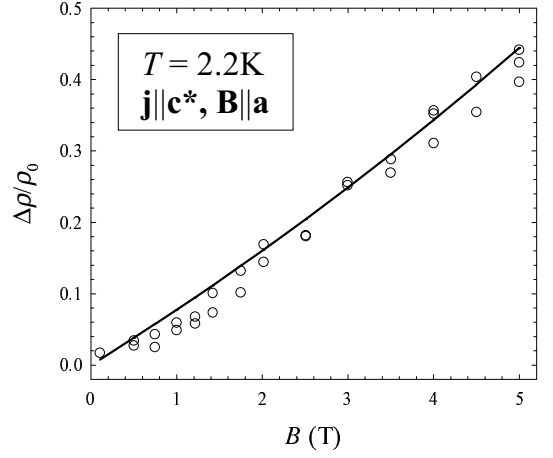


FIG. 8: Magnetic field dependence of $\Delta\rho/\rho_0$ at 2.2 K for $\mathbf{j} \parallel \mathbf{c}^*$ and $\mathbf{B} \parallel \mathbf{a}$. Solid line is fit to the theory (see text).

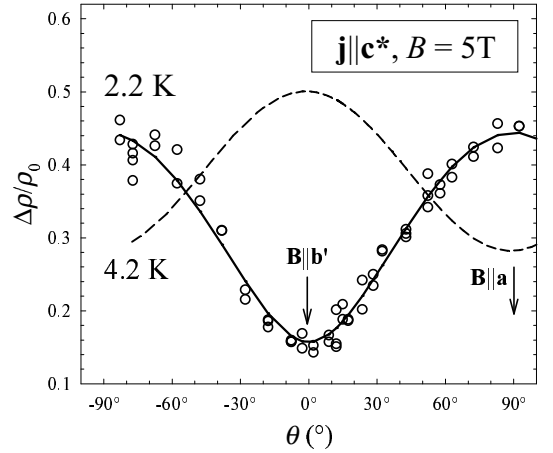


FIG. 9: Angular dependence of $\Delta\rho/\rho_0$ at 2.2 K and 4.2 K, $B = 5$ T, for $\mathbf{j} \parallel \mathbf{c}^*$, \mathbf{B} in $\mathbf{a}-\mathbf{b}'$ plane. Solid line is fit to the theory (see text).

conventional SDW where the imperfect nesting plays the crucial role. Namely, in that case we expect maxima in MR for $\mathbf{B} \parallel \mathbf{b}'$. This big change in MR anisotropy may be described within our new theoretical model. We shall compare now our experimental data at 2.2 K with the Eq. (19). The solid line is fit based on the theory that describes the data on Fig. 8 and Fig. 9 at 2.2 K very well. We deduce $A_3 = 0.0165 \text{ T}^{-1}$, $C_3 \approx 0$, and $\gamma_3 = 0.154$. From A_3 we obtain:

$$\frac{\tilde{v}_a \tilde{v}_c}{\tilde{\Delta}^2} = \xi_a \xi_c = 1.087 \times 10^{-13} \text{ cm}^2$$

and assuming $\xi_c/\xi_a = 1/13.6$ we obtain $\xi_a = 1.2 \times 10^{-6} \text{ cm}$ which is quite reasonable.² On the other hand $\gamma_3 = 0.154$ gives $\Delta_1/\Delta = 1.75$ that is too large, at least by a factor of 2, giving $\Delta_1 \approx 60$ K.

IV. CONCLUDING REMARKS

We have proposed that the phase transition at $T^* \approx 4$ K in $(\text{TMTSF})_2\text{PF}_6$ is due to the appearance of the USDW in addition to the already existing SDW. As we have shown, the quasiparticle spectrum in SDW with imperfect nesting and/or USDW in a magnetic field is, due to the Landau quantization, very different from the one for $B = 0$. The appearance of USDW order parameter modifies the quasiparticle spectrum. This change is readily accessible to both the magnetoresistance and the angular dependence of the magnetoresistance. Indeed, USDW describes the dramatic change in the magnetoresistance below $T^* \approx 4$ K. Furthermore, from the angular dependence of the magnetoresistance we can deduce the parameters $\Delta = 20$ K, $v_a/\Delta = \xi_a = 1.2 \times 10^{-6}$ cm, and $v_c/v_a = 7.33 \times 10^{-2}$, which are consistent with the previously known values. However, the new order parameter Δ_1 , associated with USDW, appears to behave somewhat

unexpectedly (as the deduced values give $\Delta_1 = 20$ K, 1 K, and 60 K for \mathbf{B} in the $\mathbf{a}-\mathbf{c}^*$ plane, in the $\mathbf{b}'-\mathbf{c}^*$ plane and in the $\mathbf{a}-\mathbf{b}'$ plane, respectively). The reason for differences of Δ_1 is unclear at present. We note, however, that in contrast to our earlier analysis,¹³ here we have taken into account the Landau quantization of the quasiparticle spectrum, but we have considered the \mathbf{k} -independence of the scattering rate. We can only suppose, that in addition to the Landau quantization the inclusion of the \mathbf{k} -dependent Γ would solve this Δ_1 discrepancy.

Acknowledgments

This experimental work was performed on samples prepared by K. Bechgaard. We thank P. Thalmeier for drawing our attention to Ref. 26 and 16. We acknowledge useful discussions with A. Hamzić and S. Tomić.

-
- * Electronic address: basletic@phy.hr
- ¹ D. Jérôme, A. Mazaud, M. Ribault, and K. Bechgaard, *J. Phys. (Lettres)* **41**, L95 (1980).
 - ² T. Ishiguro, K. Yamaji, and G. Saito, *Organic superconductors* (Springer, 1998), 2nd ed.
 - ³ I. J. Lee, S. E. Brown, W. G. Clark, J. Strouse, M. J. Naughton, W. Kang, and P. M. Chaikin, *Phys. Rev. Lett.* **88**, 017004 (2002).
 - ⁴ T. Takahashi, Y. Maniwa, H. Kawamura, and G. Saito, *J. Phys. Soc. Jpn.* **55**, 1367 (1986).
 - ⁵ T. Takahashi, T. Harada, Y. Kobayashi, K. Kanoda, K. Suzuki, K. Murata, and G. Saito, *Synth. Metals* **41-43**, 3985 (1991).
 - ⁶ J. C. Lasjaunias, K. Biljaković, F. Nad', P. Monceau, and K. Bechgaard, *Phys. Rev. Lett.* **72**, 1283 (1994).
 - ⁷ S. Tomić, N. Biškup, and A. Omerzu, *Synth. Metals* **85**, 1597 (1997).
 - ⁸ M. Basletic, A. Hamzić, B. Korin-Hamzić, and K. Bechgaard, *Synth. Metals* **103**, 2044 (1999).
 - ⁹ B. Korin-Hamzić, M. Basletic, N. Francetić, A. Hamzić, and K. Bechgaard, *J. Phys. IV France* **9**, Pr10:247 (1999).
 - ¹⁰ B. Korin-Hamzić, M. Basletic, A. Hamzić, K. Bechgaard, and M. Nagasawa, *Synth. Metals* **120**, 833 (2001).
 - ¹¹ S. Kagoshima, Y. Saso, M. Maesato, R. Kondo, and T. Hasegawa, *Solid State Commun.* **110**, 479 (1999).
 - ¹² J. C. Lasjaunias, K. Biljaković, D. Starešinić, P. Monceau, S. Takasaki, J. Yamada, S. Nakatsuji, and H. Anzai, *Europhys. J. B* **7**, 541 (1999).
 - ¹³ B. Korin-Hamzić, M. Basletic, and K. Maki, *Europhys. Lett.* **43**, 450 (1998).
 - ¹⁴ X. Huang and K. Maki, *Phys. Rev. B* **40**, 2575 (1989).
 - ¹⁵ B. Dora and A. Virosztek, *Europhys. J. B* **22**, 167 (2001).
 - ¹⁶ A. A. Nersesyan, G. I. Japaridze, and I. G. Kimeridze, *J. Phys. Cond. Matt.* **3**, 3353 (1991).
 - ¹⁷ H. Ikeda and Y. Onashi, *Phys. Rev. Lett.* **81**, 3723 (1998).
 - ¹⁸ L. Benfatto, S. Caprara, and C. D. Castro, *Eur. Phys. J. B* **17**, 95 (2000).
 - ¹⁹ S. Chakraverty, R. B. Laughlin, D. K. Morr, and C. Nayak, *Phys. Rev. B* **63**, 094503 (2001).
 - ²⁰ M. Basletic, B. Korin-Hamzić, M. V. Kartsovnik, and H. Müller, *Synth. Metals* **120**, 1021 (2001).
 - ²¹ B. Dora, A. Virosztek, and K. Maki, *Phys. Rev. B* **64**, 041101(R) (2001).
 - ²² A. Virosztek, K. Maki, and B. Dora, cond-mat/0112387.
 - ²³ B. Korin-Hamzić, M. Basletic, and K. Maki, submitted to *Int. J. Mod. Phys. B*.
 - ²⁴ J. R. Cooper, L. Forró, and B. Korin-Hamzić, *Mol. Cryst. Liq. Cryst.* **119**, 121 (1985).
 - ²⁵ K. Bechgaard, C. S. Jacobsen, K. Mortensen, J. H. Pederson, and N. Thorup, *Solid State Commun.* **33**, 1119 (1980).
 - ²⁶ A. A. Nersesyan and G. E. Vachnadze, *J. Low. Temp. Phys.* **77**, 293 (1989).